Volume 15 | Number 7 | 21 February 2019 | Pages 1459–1694

Soft Matter

rsc.li/soft-matter-journal

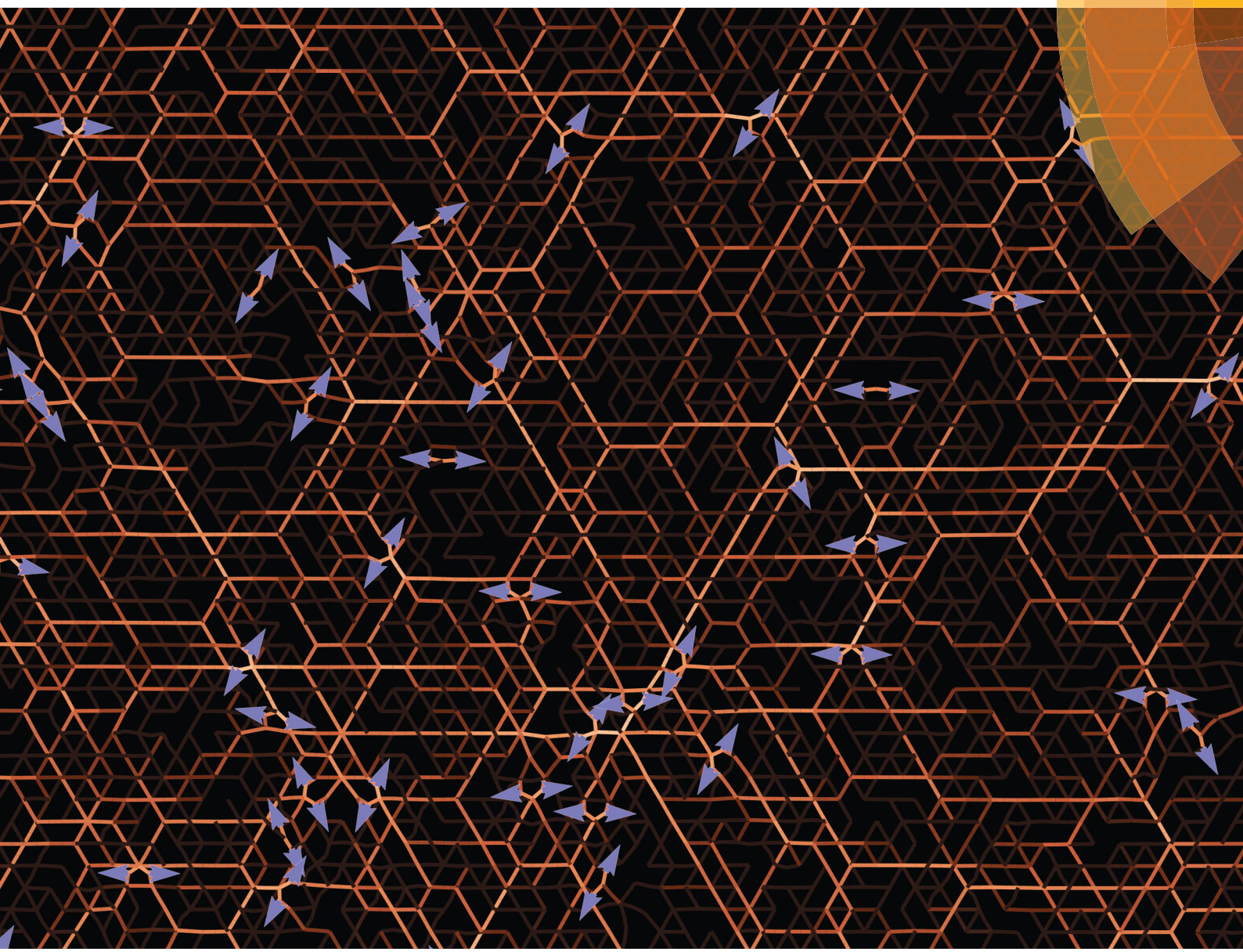

ISSN 1744-6848

ROYAL SOCIETY OF CHEMISTRY | Celebrating IYPT 2019

PAPER
Martin Lenz *et al.*
Fiber plucking by molecular motors yields large emergent contractility in stiff biopolymer networks

Soft Matter

PAPER

Check for updates

Cite this: *Soft Matter*, 2019, **15**, 1481

Fiber plucking by molecular motors yields large emergent contractility in stiff biopolymer networks

Pierre Ronceray,[a] Chase P. Broedersz[b] and Martin Lenz*[cd]

Received 12th May 2018,
Accepted 18th December 2018

DOI: 10.1039/c8sm00979a

rsc.li/soft-matter-journal

The mechanical properties of the cell depend crucially on the tension of its cytoskeleton, a biopolymer network that is put under stress by active motor proteins. While the fibrous nature of the network is known to strongly affect the transmission of these forces to the cellular scale, our understanding of this process remains incomplete. Here we investigate the transmission of forces through the network at the individual filament level, and show that active forces can be geometrically amplified as a transverse motor-generated force "plucks" the fiber and induces a nonlinear tension. In stiff and densely connected networks, this tension results in large network-wide tensile stresses that far exceed the expectation drawn from a linear elastic theory. This amplification mechanism competes with a recently characterized network-level amplification due to fiber buckling, suggesting that that fiber networks provide several distinct pathways for living systems to amplify their molecular forces.

I Introduction

Living organisms use chemical energy to produce the mechanical forces required to move and control their shape. These forces originate at the molecular scale from the power strokes exerted by molecular motors, and are generically transmitted by fiber networks such as the actin cortex, thus resulting in large-scale stresses.[1] To develop a theory for active stress generation allowing to both infer microscopic behaviors from large-scale stresses and to predict the latter from the former, it is thus important to understand both how active forces exerted on an individual filament transmit along this filament to the mesh size level, and are subsequently propagated through the network. Stress generation thus involves force transmission through local one-dimensional objects and higher-dimensional networks.

Tensile forces propagating through such biopolymer networks can be much longer-ranged than would be expected from linear elastic force transmission,[2–6] and have been proposed to enhance cell–cell mechanical communication.[7] This suggests that fiber networks do more than simply transmitting forces: they amplify them.[8] This amplification of contractile stresses can be accounted for by the large-scale mechanical response of the network surrounding the motors. There, buckling of filaments under compression increases the range of propagation of tensile forces, thus enhancing contractile stresses. In order to generate a significant amplification, this scenario requires active forces that are much larger than the buckling force of individual filaments, which induce buckling in a large neighborhood of the motor. As a result, this mechanism for stress generation is sensitive to the network's mechanical properties and results in very limited amplification in stiff, densely connected networks.

Here we investigate another stress amplification mechanism, also based on mechanical equilibrium considerations, that becomes dominant in such stiff networks. This mechanism involves force transmission at smaller scales than the previous one, and we thus consider how forces exerted by a motor on a filament are transmitted by this filament to the rest of the network (Fig. 1a and b). When subjected to a sufficiently large longitudinal motor force, the filament buckles, which at this single-filament level results in a limited force amplification (Fig. 1c). By contrast, a filament under a transverse active force deforms and tenses as a plucked string (Fig. 1d), an effect for which we introduce a single-filament model in Section II. In this geometry, the force transmitted to the mesh size level consists of the initial active force, plus an additional contractile force dipole due to this plucking tension. In Section III, we show that this plucking-induced contractility can become much larger than the one naively expected from the magnitude of the motor force, thus leading to force amplification at the level of a single filament.

[a] *Princeton Center for Theoretical Science, Princeton University, Princeton, NJ 08544, USA*
[b] *Arnold-Sommerfeld-Center for Theoretical Physics and Center for NanoScience, Ludwig-Maximilians-Universität München, D-80333 München, Germany*
[c] *LPTMS, CNRS, Univ. Paris-Sud, Université Paris-Saclay, 91405 Orsay, France. E-mail: martin.lenz@u-psud.fr*
[d] *MultiScale Material Science for Energy and Environment, UMI 3466, CNRS-MIT, 77 Massachusetts Avenue, Cambridge, Massachusetts 02139, USA*

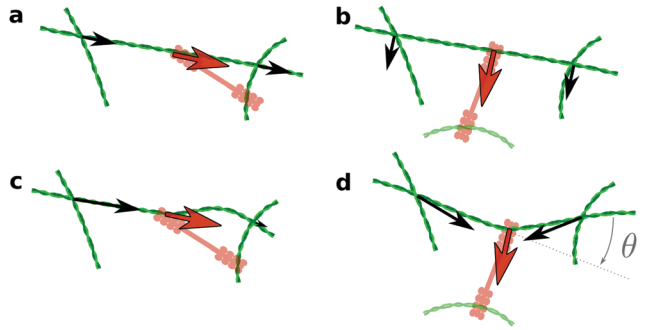

Fig. 1 Local response of actin filaments to myosin forces. (a and b) Linear response of a filament to an active force F (red arrow) exerted by a motor along and perpendicular to the filament, respectively. Black arrows show the forces transmitted by the filament to the rest of the network. (c) A large force along the filament leads to buckling of the compressed part. This effectively results in adding a contractile tension T_{buckle} in the filament, the magnitude of which is bounded by the motor force ($T_{\text{buckle}} \lesssim F$). (d) A force exerted perpendicularly to the filament tenses it, as does a musician plucking the string of their instrument. Assuming the angular deflection θ of the filament remains small, this geometrical effect results in a tension $T_{\text{pluck}} \sim F/\theta$ along the filament's direction which can be much larger than the applied force. The rigidity of the surrounding network is crucial for this amplification mechanism, as θ can only remain small if the filament is firmly anchored at its ends.

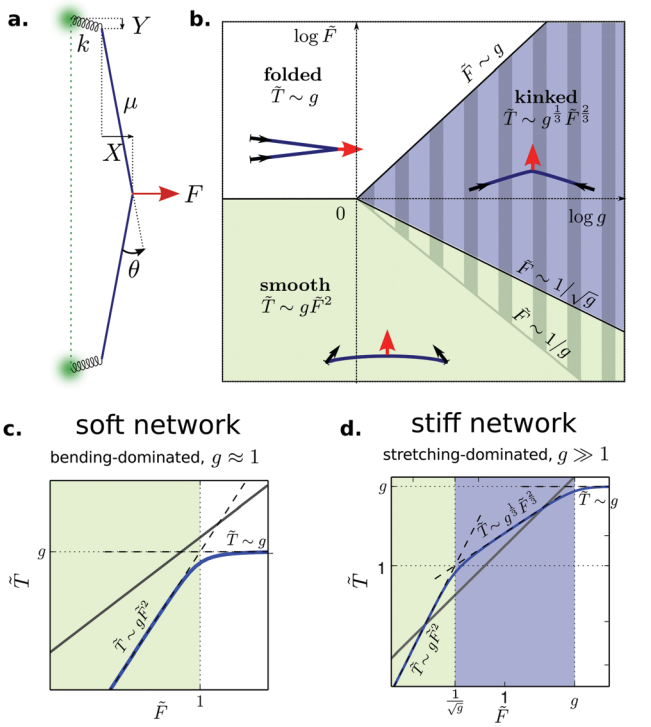

Fig. 2 Single-filament model for filament plucking. (a) Model notation, as introduced in eqn (1). (b) Scaling regimes for the dimensionless nonlinear tension $\tilde{T}$ that a plucked filament transmits to the surrounding network, as a function of the dimensionless plucking force $\tilde{F}$ and the effective stretch-to-bend rigidity g of the system defined in eqn (9). Filled areas indicate different scaling regions: smooth (green), kinked (blue) and folded (white), with inset depicting each situation. The hatched area represents the domain of parameters where the plucking tension T exceeds the applied force F, indicating that plucking dominates the forces transmitted to the network. (c) The plucking tension (blue line, obtained by minimizing the energy in eqn (1)) as a function of the active force for a soft network with $g = 1$; this tension never exceeds the applied force F (gray line), and the kinked regime does not appear. (d) In a stiff network, $g \gg 1$, all three regimes are present, with a wide regime of force amplification where the blue line is above the grey line.

This geometrical effect is controlled by the deflection angle of the filament, which in turn depends on the stiffness of both the filament and the network: the stiffer the network, the smaller the deflection, the larger the amplification. By explicitly modeling fiber networks involving many filaments, we show in Section IV that this results in a strong dependence of the amplification on the network connectivity, which itself controls its stiffness.[9] This study complements our understanding of network-level force amplification, and should be included in a comprehensive theory for force amplification in biopolymer networks.

II A single-filament model for fiber plucking

To account for the large tensions induced in a filament as a "plucking" force is exerted perpendicular to it, we introduce a single-filament model illustrated in Fig. 2a. The plucked fiber consists of two hinged rods acting under extension as Hookean springs with rest length ℓ_0 and spring constant μ, which models the entropic elasticity of the semiflexible fiber. Anticipating on our later results, plucking will be especially effective on filaments with a large μ. An active force F is exerted perpendicular to the filament at the hinge, modeling the action of a molecular motor on this filament. Note that force balance imposes that this motor exerts an opposite force on another filament. We penalize any bending of the filament by an angle θ with an energy $2\kappa \sin^2(\theta/2)$. The exact form of this penalty is unimportant as long as it goes as $\kappa\theta^2/2$ for small angles, which implies that the filament's bending modulus is κ. The surrounding network is modeled as two additional zero-length Hookean springs with spring constant k anchoring the filament to a fixed substrate. The state of the filament is thus represented by two geometrical coordinates X and Y, which respectively characterize the filament bending deformation and the network deformation. The energy of the system reads:

$$E = \underbrace{-FX}_{\text{active force}} + \underbrace{\left[\mu(\delta\ell)^2 + 2\kappa \sin^2\frac{\theta}{2}\right]}_{\text{filament deformation}} + \underbrace{kY^2}_{\text{network response}} \qquad (1)$$

with $\delta\ell = \sqrt{X^2 + (\ell_0 - Y)^2} - \ell_0$ and $\tan(\theta/2) = X/(\ell_0 - Y)$. In practice, actin filaments are much easier to bend than to stretch, implying $\mu\ell_0^2 \gg \kappa$. Note that in eqn (1) we do not consider the bulk translation of the filament along the force direction, which is fully set by force balance and thus decouples from the mechanical properties of the filament.

Our description includes a static motor in a mechanically equilibrated static network, which is correct on times scales much longer than the mechanical equilibration time of the

This journal is © The Royal Society of Chemistry 2019

network (microseconds to milliseconds), and much smaller than the time scales associated with motor and crosslinker binding/unbinding as well as filament assembly/disassembly (typically seconds to minutes). On longer time scales, the contractility of the network results from a succession of events where motors bind to the network, transiently exert the tension discussed here, then release their hold. The magnitude of these pulling events, which we study here, thus directly determines the steady-state tension of the network.

III Force amplification at the single filament level

To elucidate the magnitude of the contraction generated by our single-filament model, we compute the tensile force $T = kY$ that it transmits to the rest of the network in the vertical direction, and compare its magnitude to that of the applied force F: an amplification ratio T/F larger than one implies that the plucking-induced tension dominates the force transmitted to the network. While the force in the horizontal direction also contributes to the contractility of the network, we do not discuss it further as it is always equal to F due to force balance and thus cannot be amplified. We first consider the case where the response of the system to the active force has a small amplitude, *i.e.* when both $X \ll \ell_0$ and $Y \ll \ell_0$. In this regime we have

$$\delta\ell \approx \frac{X^2}{2\ell_0} - Y \quad \text{and} \quad \sin\frac{\theta}{2} \approx \frac{X}{\ell_0} \tag{2}$$

We can thus rewrite the energy:

$$E = \underbrace{-FX}_{\text{applied force}} + \underbrace{\mu\left(\frac{X^2}{2\ell_0} - Y\right)^2}_{\text{filament stretching}} + \underbrace{\frac{2\kappa X^2}{\ell_0^2}}_{\text{filament bending}} \quad \underbrace{kY^2}_{\text{network response}}. \tag{3}$$

Minimizing this energy yields:

$$\frac{\partial E}{\partial X} = 0 = -F + \frac{\mu X}{\ell_0}\left(\frac{X^2}{\ell_0} - 2Y\right) + \frac{4\kappa X}{\ell_0^2} \tag{4}$$

$$\frac{\partial E}{\partial Y} = 0 = -\mu\left(\frac{X^2}{\ell_0} - 2Y\right) + 2kY. \tag{5}$$

The second equation implies

$$Y = \frac{\mu X^2}{2\ell_0(\mu + k)} \tag{6}$$

and thus, substituting this value in eqn (4), we have:

$$F = \frac{\mu k}{2\ell_0^2(\mu + k)}X^3 + \frac{4\kappa X}{\ell_0^2}, \tag{7}$$

which we can rewrite in a dimensionless form as

$$\frac{\ell_0}{4\kappa}F = g\frac{X^3}{\ell_0^3} + \frac{X}{\ell_0}. \tag{8}$$

Here the role of the filament stretching modulus μ and bending modulus κ and the network stiffness k are combined in a single dimensionless parameter

$$g = \frac{\mu k \ell_0^2}{4\kappa(\mu + k)} \approx \min(k, \mu) \times \frac{\ell_0^2}{4\kappa}, \tag{9}$$

which corresponds to an effective stretching-to-bending rigidity ratio of the system, *i.e.* that associated with the softest mode of stretching deformation, either that of the network or that of the filament. Going to dimensionless units, we define a dimensionless force

$$\tilde{F} = \frac{\ell_0}{4\kappa}F. \tag{10}$$

Similarly we define the dimensionless tension $\tilde{T} = T\ell_0/8\kappa$ where $T = kY$ is the tension in the filament (note the difference of a factor two in scale between force and tension, chosen to absorb numerical prefactors from following expressions). Due to the left-right symmetry of Fig. 2a, the tension in the filament is even in the force, and thus has the nonlinear dependence $\tilde{T} \approx g(X/\ell_0)^2$ in the small elongation limit $\delta\ell \ll \ell_0$. We can thus rewrite eqn (7) in terms of the dimensionless tension and force:

$$g^{1/2}\tilde{F} = \tilde{T}^{1/2}(1 + \tilde{T}) \tag{11}$$

which relates the plucking tension to the applied force and the mechanical properties of the system. As a result, in the small-displacement regime the value of the plucking tension depends on the system parameters only through the combination $g^{1/2}\tilde{F}$.

Now considering both small and large displacements, we distinguish between the three amplification regimes illustrated in Fig. 2b, the first two being directly described by eqn (11):

- at small forces $\tilde{F} \ll g^{-1/2}$, the filament's response is dominated by its bending stiffness, and

$$\tilde{T} \approx g\tilde{F}^2 \tag{12}$$

In this regime, the filament is bent smoothly. If our discrete filament mode were replaced by a continuum one, the same scaling would be obtained and the curvature would be spread over the whole length of the filament.

- at intermediate forces $g^{-1/2} \ll \tilde{F} \ll g$, the response is dominated by the stretching properties of the filament, and

$$\tilde{T} \approx g^{1/3}\tilde{F}^{2/3} \tag{13}$$

note that this non-trivial scaling regime only occurs if $g \gg 1$, *i.e.* for a stiff filament in a stiff network. The filament is kinked at the hinge in this regime. In a continuum filament with a stretching modulus determined by entropic elasticity, this kink would manifest itself as a localization of the curvature in a region of size $\propto (k_B T/F)^{2/3}\ell_p^{1/3}$ around the point of application of the force, where ℓ_p is the filament persistence length.[10]

- at very large force (or for a very soft network) $\tilde{F} \gg g$, the filament folds around its hinge and bends completely; in that case the plucking tension saturates to a finite value

$$\tilde{T} \approx g \tag{14}$$

that is independent of the force $\tilde{F}$.

To determine whether the effects considered here generate force amplification, we compare the magnitude of the tension T to that of the force F applied by the motor. Amplification occurs in both the smooth and kinked regimes, and specifically for $1/g \ll \tilde{F} \ll g$ as represented by the hatched area in Fig. 2b. The force amplification ratio $\tilde{T}/\tilde{F}$ reaches its maximum $\approx \sqrt{g}/2$ at the crossover between these two regimes (the asymptotes intersect at an amplification ratio of $\sqrt{g}$; the factor $\approx 1/2$ is due to the smoothness of the crossover, and varies slightly with g). At this crossover we have $\tilde{T} = 1$, meaning that the tension equals the longitudinal force required to buckle the filament.

IV Transmission of plucking forces through full networks

While we have introduced the network rigidity k as independent from the characteristics of the filament of interest, the filaments constituting the network itself are of the same nature as that filament, which strongly constrains the value of the rigidity parameter g. There is some freedom in setting the value of g however, as the elasticity of fiber networks is not only controlled by the rigidity of its components, but also by its architecture, and in particular its connectivity. Indeed, densely connected networks primarily deform through stretching modes and have $k \sim \mu$, while loosely connected networks deform through bending modes, and thus have[11] $k \sim \kappa/\ell_0^2$. Here we investigate how these different architectures impact force amplification through plucking.

Going back to our single-filament model, we predict that in soft bending-dominated networks with $g \sim 1$, the plucking tension is small compared to the applied force, regardless of the value of $\tilde{F}$ (Fig. 2c). In contrast, for stretching-dominated networks with $k \sim \mu$ (and thus $g \sim \mu\ell_0^2/4\kappa \gg 1$), there is a vast regime of force values for which amplification occurs (Fig. 2d).

To put this simple picture to the test, we simulate full networks using a numerical model where filaments are positioned at the edges of a regular two-dimensional lattice. Similar to the model of Fig. 2a, here all filaments are modeled by hinged Hookean springs of unit rest length $\ell_0 = 1$, with a stretching energy $\mu(\delta\ell)^2/2$ associated with an elongation $\delta\ell$ and a bending penalty $2\sin^2(\theta/2)$ for creating an angular deflection θ between two consecutive, initially aligned springs (*i.e.* $\kappa = 1$). In addition to their hinges at the lattice nodes, filaments have an additional hinge in between lattice nodes similar to that pictured in Fig. 2a, implying that they buckle if subjected to a longitudinal compressive force larger than the critical force $F_{\text{buckling}} = 1$. Distinct filaments are connected at each lattice vertex by crosslinks that do not constrain their relative angles. The energy is minimized with respect to the position of all nodes using the Broyden–Fletcher–Goldfarb–Shanno algorithm.[12] The critical connectivity delimiting the bending- and stretching dominated regimes discussed above can be estimated through a simple constraint counting argument, which indicates that networks where each vertex has more than $z = 4$ neighbors in two dimensions are stretching-dominated, where those with lower connectivity are bending-dominated.[9] Here we simulate one network characteristic of each regime: a high-connectivity ($z = 6$), stretching-dominated triangular lattice (Fig. 3a and b), and a low-connectivity ($z = 3$), bending-dominated network illustrated in Fig. 3c and d and further described in Appendix A.

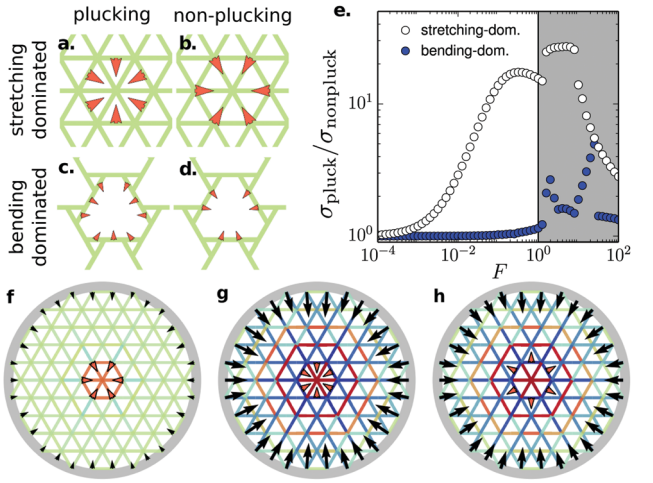

Fig. 3 Full-network model of plucking. (a–d) Local force application geometries. (e) Ratio of the stresses generated in the presence *vs.* absence of plucking in a circular stretching- (bending-)dominated network with radius $R = 11$. In the gray area buckling occurs, resulting in large displacements and a complex network response involving the effects described in ref. 8. (f and g) Force propagation in a stretching-dominated network in the non-plucking and plucking geometries, respectively, at force $\tilde{F} = 0.05$. Blue (red) bonds are under tension (compression). Black arrows indicate forces at a fixed boundary. (h) Reversing forces compared to the previous panel leaves the stress pattern almost unchanged. Active force and stress scale are the same in panels f–h. Boundary forces are magnified 5 times in panel f. for legibility. In all simulations $\mu = 10^4$.

To quantify the amount of contractile tension induced by a single motor in a circular piece of network with fixed boundaries, we measure the isotropic part of the coarse-grained macroscopic contractile stress (corresponding to the "active stress" of active gel theories[13,14]), which reads[15]

$$\sigma = -\frac{1}{V}\sum_i \mathbf{f}_i \cdot \mathbf{r}_i \qquad (15)$$

where V is the system's volume, the sum runs over the vertices that belong to the boundary of the network, and $\mathbf{f}_i$ is the force exerted on the boundary at node i located at position $\mathbf{r}_i$. To assess the contribution of plucking to this contractile stress, we compare situations with and without plucking. The former situation is illustrated in Fig. 3a and c, the motor forces are exerted at the midpoint of each filament. The latter corresponds to forces being applied to the lattice vertices as shown in Fig. 3b and d. We plot the ratio $\sigma_{\text{pluck}}/\sigma_{\text{nonpluck}}$ of contractile stresses in the two situations in Fig. 3e. For bending-dominated networks, it is roughly equal to one for all force values, indicating that plucking is of little relevance in these systems, as predicted by our local calculation (Fig. 2c). In contrast, in stretching-dominated networks the plucking contribution is large, with a stress ratio culminating at a large value ≈ 17.

This journal is © The Royal Society of Chemistry 2019

This value is compatible with the expectation drawn from our one-filament model, which predicts an amplification of the order of $\sqrt{g}/2$, with $\sqrt{g} \approx \sqrt{\mu/8} \approx 18$ here since $\mu \approx k$. This strong amplification is evident when comparing Fig. 3f and g, showing the force transmission pattern in the stretching-dominated network with forces applied in a non-plucking and plucking geometry, respectively. The macroscopic stress of the latter system is 17 times larger than that of the former.

The plucking tension is intrinsically contractile in simple networks, as plucking a filament always tends to shorten its end-to-end distance. As a result, the far-field plucking stress does not depend on the orientation of the force perpendicular to the filament, but only on its magnitude. We illustrate this by reversing the active forces of Fig. 3g in Fig. 3h without any significant alteration of the force transmission pattern. As a result, plucking results in a reversal of locally extensile forces into far-field contractile forces, reminiscent of the buckling-induced rectification reported in ref. 8.

The results presented in Fig. 3 are not specific to regular geometries or two-dimensional networks. Indeed, we demonstrate in Fig. 4 that they robustly extend to disordered three-dimensional networks. Here we use a face-centered cubic (FCC) lattice and control the connectivity by randomly depleting the network, keeping each lattice edge with a probability p. For $p > 0.47$, such networks are stretching-dominated, while for $0.27 < p < 0.47$ they are bending-dominated.[9] We model active forces as randomly located force dipoles, exerted either at mid-edges (plucking geometry, Fig. 4a) or on lattice vertices (non-plucking geometry, Fig. 4b). The ratio of the macroscopic active stress between these two geometries is plotted in Fig. 4c. As in the regular network case (Fig. 3e), this ratio shows no increase in bending-dominated networks with increasing force. In contrast, it reveals a plucking amplification of up to 30× in stretching-dominated at intermediate forces, consistently with our analysis.

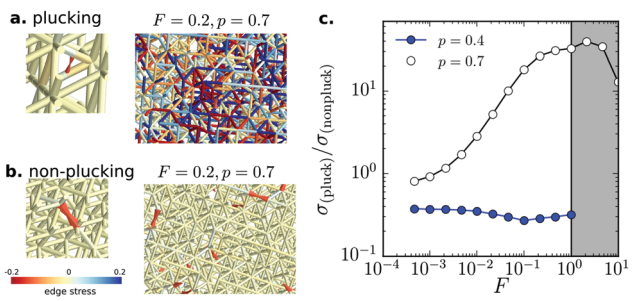

Fig. 4 Response of a disordered three-dimensional fiber network to force dipoles. (a) With plucking (dipole forces exerted at mid-edges), and (b) without plucking (forces at lattice vertices). Left: Geometry of force exertion. Right: Response of the network. Color indicates the state of stress of the bonds. (c) Ratio of the stress in the plucking and non-plucking network at equal force, for a bending-dominated (blue, p = 0.4) and stretching-dominated network (white, p = 0.7). In the gray area buckling occurs; for bending-dominated networks this results in the collapse of contractile dipoles and prevents further increase of the force. Parameters: 10^3 sites FCC lattice; 50 force dipoles; periodic boundary conditions (stress is measured using the mean-stress theorem as in ref. 8); $\mu = 10^4$.

V Discussion

Our results show that the generation of large-scale active stress σ in stiff biopolymer networks depends not only on the magnitude F of the local active forces, but also crucially on the geometry of force exertion. Forces exerted at filament intersections or along filaments induce a linear stress response $\sigma \propto F$ if the force is smaller than the filaments' buckling threshold. In contrast, forces exerted with a perpendicular component to a filament, far from filament intersections, can induce a strongly nonlinear stress response even for forces well below this threshold. The tension resulting from this geometrical effect, which we term plucking, can dominate the far-field response, strongly amplify contractile stresses and reverse locally extensile forces. This plucking effect is generic and independent of spatial dimension.

While plucking can amplify stresses by over an order of magnitude for biologically relevant parameters, it involves several requirements. First, it requires moderate forces, sufficient to bend the filament that they are applied to but not large enough to fold it or buckle its neighbors (Fig. 3e). Second, these forces need to be applied sufficiently far from network cross-links and have a component perpendicular to the filament. While we do not discuss the microscopic mechanism by which molecular motors exert forces on cytoskeletal filaments in this article, we note that these conditions are compatible with our current understanding of actin–myosin interactions.[10] Third, plucking necessitates a stiff, densely connected network of flexible filaments, and is negligible in softer, bending-dominated gels. This point was missed in previous studies of local motor-induced network deformations.[10] Beyond the linear networks considered here, stiffening under stress, both at the level of individual biopolymers and of whole gels, could thus enhance stress amplification by plucking.

Plucking is distinct from buckling as a stress amplification mechanism, although they share some characteristics. Indeed, both are nonlinear single-filament effects that rectify all local forces towards contraction while strongly amplifying far-field stresses. These effects are each characterized by specific signatures that could be experimentally assessed to determine their individual pertinence. Plucking amplifies forces at a purely local level, making it highly sensitive to the local geometry of force exertion. The resulting amplification culminates at intermediate force and increases in magnitude with network stiffness. Buckling, in contrast, is essentially insensitive to local geometry. At larger scales however, buckling nonlinearly amplifies stress through an increased range of force transmission – as in a rope network, rather than an elastic medium. This amplification always increases with increasing force, but decreases with increasing network stiffness as filament buckling becomes more difficult. Despite their differences, buckling and plucking can cooperate: the large local forces emerging from plucking in the kinked regime exceed the buckling threshold, and are thus further amplified by buckling the surrounding network through force transmission.

In cells, the magnitude of plucking-induced amplification could be controlled by varying the mesh size of the actin cytoskeleton.

Remembering that $\mu \sim k_B T \ell_p^2/\ell_0^4$ and $\kappa \sim k_B T \ell_p/\ell_0$, where $k_B T$ is the thermal energy and ℓ_p the persistence length of a filament,[11] the smooth, kinked and folded regimes respectively imply $T \propto \ell_0$, $T \propto \ell_0^{-1}$ and $T \propto \ell_0^{-3}$. As a result, at large forces plucking-induced amplification should decrease with increasing mesh size, in contrast with buckling-induced amplification. Another factor influencing the effective rigidity of the actin cytoskeleton is its possible interconnection with intermediate filaments, which can rigidify it significantly.[16–18] The cell could thus modulate the relative role of plucking- and buckling-induced amplification by regulating the coupling between the actin and intermediate filament cytoskeletons. By artificially modulating the properties of the latter, one could also experimentally determine which amplification mechanism dominates in a given cellular context.

A similar strategy could be used in an *in vitro* experiment to determine which of these two—if any—mechanisms dominates. One could thus study reconstituted 2D actomyosin networks anchored on an elastic gel, whose stress could be measured by traction force microscopy. Increasing the concentration of anchor points between the network and the substrate would increase the stiffness of the gel, while leaving its structure unchanged: in a buckling-dominated scenario, this would thus reduce the tension, while the stress would increase if it resulted mostly from plucking.

Plucking and buckling thus provide distinct routes to amplify biological forces. Buckling amplifies forces at any strain, allowing cells in the extracellular matrix to enhance stress transmission and modify the mechanical properties of the matrix over large distances.[19] Plucking, in contrast, generates large stresses only at small strains. It could thus help build tension in the cells actomyosin cortex. Plucking has been directly observed in reconstituted actomyosin networks,[20] and we hope our study will help design experiments to directly assess its contribution to cell mechanics.

Conflicts of interest

There are no conflicts to declare.

Appendix A: a regular bending-dominated network geometry

As described in the main text, fiber networks explore different elastic regimes depending on their average connectivity. While these different regimes have previously been studied in disordered networks,[9] here we avoid the technical difficulties associated with disorder by designing a minimal regular, bending-dominated sublattice of the triangular lattice. Its local structure is illustrated in Fig. 3c and d of the main text. To further characterize the structure and elasticity of this network, we describe its elastic and geometrical response to shear and dilation strain in Fig. 5. All deformation modes presented show non-affine deformations characteristic of bending-dominated networks. As expected for a bending-dominated network, the network's elastic moduli are of order one, *i.e.*, on par with the filament bending rigidity. By contrast, the moduli of a highly coordinated, stretching-dominated triangular network are of order $\mu \gg 1$.

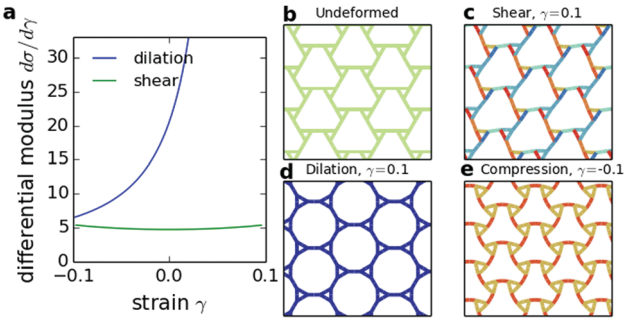

Fig. 5 Elasticity and geometry of a minimal bending-dominated network. (a) Macroscopic stress–strain curves under bulk dilation and shear. (b) The network in the undeformed configuration. (c) Response to shear. (d) Response to uniform dilation. (e) Response to uniform compression. Red: compressed bonds, blue: tense bonds. Filament stretching modulus $\mu = 10^3$.

Acknowledgements

This work was supported by a PCTS fellowship to PR, the German Excellence Initiative *via* the program "NanoSystems Initiative Munich" (NIM) and the Deutsche Forschungsgemeinschaft (DFG) *via* the GRK2062/1 to CPB, Marie Curie Integration Grant PCIG12-GA-2012-334053, "Investissements d'Avenir" LabEx PALM (ANR-10-LABX-0039-PALM), ANR grant ANR-15-CE13-0004-03 and ERC Starting Grant 677532 to ML. ML's group belongs to the CNRS consortium CellTiss. PR is supported by a Philippe Foundation travel grant.

References

1 L. Blanchoin, R. Boujemaa-Paterski, C. Sykes and J. Plastino, Actin Dynamics, Architecture, and Mechanics in Cell Motility, *Physiol. Rev.*, 2014, **94**, 235–263.
2 Y. Shokef and S. A. Safran, Scaling Laws for the Response of Nonlinear Elastic Media with Implications for Cell Mechanics, *Phys. Rev. Lett.*, 2012, **108**(17), 178103.
3 J. Notbohm, A. Lesman, P. Rosakis, D. A. Tirrell and G. Ravichandran, Microbuckling in fibrin networks enables long-range cell mechanosensing, *J. R. Soc., Interface*, 2015, **12**(108), 20150320.
4 P. Rosakis, J. Notbohm and G. Ravichandran, A model for compression-weakening materials and the elastic fields due to contractile cells, *J. Mech. Phys. Solids*, 2015, **85**, 16–32.
5 X. Xu and S. A. Safran, Nonlinearities of Biopolymer Gels Increase the Range of Force Transmission, *Phys. Rev. E: Stat., Nonlinear, Soft Matter Phys.*, 2015, **92**(03), 032728.
6 H. Wang, A. S. Abhilash, C. S. Chen, R. G. Wells and V. B. Shenoy, Long-range force transmission in fibrous

 This journal is © The Royal Society of Chemistry 2019

matrices enabled by tension-driven alignment of fibers, *Biophys. J.*, 2014, **107**(11), 2592–2603.
7 R. S. Sopher, H. Tokash, S. Natan, M. Sharabi, O. Shelah, O. Tchaicheeyan and A. Lesman, Nonlinear elasticity of the ECM fibers facilitates efficient inter-cellular mechanical communication, *Biophys J.*, 2018, **115**(7), 1357–1370.
8 P. Ronceray, C. Broedersz and M. Lenz, Fiber networks amplify active stresses, *Proc. Natl. Acad. Sci. U. S. A.*, 2016, **113**(11), 2827–2832.
9 C. P. Broedersz, X. Mao, T. C. Lubensky and F. C. MacKintosh, Criticality and isostaticity in fibre networks, *Nat. Phys.*, 2011, **7**, 983–988.
10 M. Lenz, Geometrical Origins of Contractility in Disordered Actomyosin Networks, *Phys. Rev. X*, 2014, **4**, 041002.
11 C. P. Broedersz and F. C. MacKintosh, Modeling semiflexible polymer networks, *Rev. Mod. Phys.*, 2014, **86**, 995–1036.
12 R. Fletcher, *Practical Methods of Optimization*, Wiley, 2000.
13 K. Kruse, J. F. Joanny, F. Jülicher, J. Prost and K. Sekimoto, Generic theory of active polar gels: a paradigm for cytoskeletal dynamics, *Eur. Phys. J. E: Soft Matter Biol. Phys.*, 2005, **16**(1), 5–16.
14 J. Prost, F. Jülicher and J. F. Joanny, Active gel physics, *Nat. Phys.*, 2015, **11**(2), 111–117.
15 P. Ronceray and M. Lenz, Connecting local active forces to macroscopic stress in elastic media, *Soft Matter*, 2015, **11**(8), 1597–1605.
16 O. Esue, A. A. Carson, Y. Tseng and D. Wirtz, A Direct Interaction between Actin and Vimentin Filaments Mediated by the Tail Domain of Vimentin, *J. Biol. Chem.*, 2006, **281**(41), 30393–30399.
17 T. Golde, C. Huster, M. Glaser, T. Händler, H. Herrmann and J. A. Käs, *et al.*, Glassy dynamics in composite biopolymer networks, *Soft Matter*, 2018, **14**, 7970.
18 M. Guo, A. J. Ehrlicher, S. Mahammad, H. Fabich, M. H. Jensen and J. R. Moore, *et al.*, The Role of Vimentin Intermediate Filaments in Cortical and Cytoplasmic Mechanics, *Biophys. J.*, 2013, **105**, 1562–1568.
19 Y. L. Han, P. Ronceray, G. Xu, A. Malandrino, R. D. Kamm, M. Lenz, C. P. Broedersz and M. Guo, Cell contraction induces long-ranged stress stiffening in the extracellular matrix, *Proc. Natl. Acad. Sci. U. S. A.*, 2018, **115**(16), 4075–4080.
20 D. S. Seara, V. Yadav, I. Linsmeier, A. P. Tabatabai, P. W. Oakes, S. M. A. Tabei, S. Banerjee and M. P. Murrell, Entropy production rate is maximized in non-contractile actomyosin, *Nat. Commun.*, 2018, **9**, 4948.